Widespread Euxinic Conditions are not a Prerequisite for Sediment-Hosted Base Metal (Pb-Zn-Ba) Mineralization at MacMillan Pass, Yukon

J.M. Magnall, R.A. Stern, and S.A. Gleeson
Department of Earth and Atmospheric Sciences, University of Alberta, Edmonton, AB, T6G 2E3
magnall@ualberta.ca

S. Paradis
Geological Survey of Canada, Box 6000, 9860 West Saanich Road, Sidney, BC, V8L 4B2

Abstract

Late Devonian strata in the MacMillan Pass District, Selwyn Basin, Yukon, are host to two Pb-Zn-Ba deposits, Tom and Jason. Mineralization has previously been considered stratiform, and base metal sulphides (pyrite-sphalerite-galena) are thought to have precipitated from the water column, along with barite. A first order control on the precipitation of sulphides, therefore, is the presence of reduced sulphur in the water column (euxinic conditions). Over 400 samples of drill core intersecting the mineralization at Tom and Jason were obtained, in order to comprehensively evaluate the textural evidence for stratiform mineralization. The mineralogy and the paragenetic relationship between barite and base metal sulphides were determined using transmitted and reflected light, and backscatter electron imaging. The paragenetic framework provided a context within which to perform in situ sulphur isotope microanalysis (secondary ion mass spectrometry; SIMS) of barite and pyrite.

In the samples from both Tom and Jason, there is strong petrographic evidence that barite formed during early diagenesis, pre-dating hydrothermal input. In addition, there are at least two generations of diagenetic pyrite associated with the barite. All hydrothermal sulphides (pyrite, sphalerite and galena) clearly post-date and overprint the diagenetic barite-pyrite assemblage. This textural evidence raises the question as to whether mineralization is truly syn-sedimentary. Diagenetic pyrite comprises two end-member isotopic populations: framboidal pyrite (*py-I*; -23‰ to -28‰), and euhedral pyrite (*py-II*; 8‰ to 26‰). Barite intergrown with *py-II* has a median $\delta^{34}S$ composition of 28‰, and a range of 24‰ to 34‰. These $\delta^{34}S_{\text{-barite}}$ values overlap with the isotopic composition of Late Devonian seawater sulphate, which rules out near quantitative reduction of seawater sulphate in the water column as a mechanism for sulphide production. In the absence of euxinic conditions, an alternative source of reduced sulphur is

Recommended citation
Magnall, J.M., Stern, R.A., Gleeson, S.A., and Paradis, S., 2015. Widespread euxinic conditions are not a prerequisite for sediment-hosted base metal (Pb-Zn-Ba) mineralization at MacMillan Pass, Yukon, *in* Paradis, S., ed., Targeted Geoscience Initiative 4: sediment-hosted Zn-Pb deposits: processes and implications for exploration; Geological Survey of Canada, Open File 7838, p. 43-57. doi:10.4095/296328

required to account for base metal sulphide accumulation in the MacMillan Pass strata; barite replacement is one potential mechanism, and is supported by substantial textural and mineralogical evidence. Further work will be required to establish its importance from a mass balance perspective.

Introduction

MacMillan Pass, Yukon, is situated approximately 390 km NE of Whitehorse, adjacent to the Northwest Territories (NT) border (Figure 1a). It is the location of important sediment-hosted Zn-Pb-(Ba) mineralization, at the mineral occurrences of Tom and Jason (Figure 1b). Mineralization is hosted within Upper Devonian Selwyn Basin strata, comprised of organic-rich, siliceous mudstones that form part of the Earn Group (Figure 2) (Gordey et al., 1982). The MacMillan Pass deposits have traditionally been viewed as type-characteristic sedimentary exhalative (SEDEX) deposits (Goodfellow and Lydon, 2007); Tom and Jason both display a clearly defined zone of hydrothermal upflow (stockwork style veining), located stratigraphically above what is considered to be bedded to laminated, stratiform base metal sulphide mineralization in overlying mudstones (Figure 3). Models for this style of mineralization in the Selwyn Basin involve syn-sedimentary precipitation of base metal sulphides from the water column following hydrothermal venting (Goodfellow, 2007). A prerequisite for effective base-metal precipitation is therefore basinal euxinia, i.e. the buildup of H_2S in the water column, at the expense of bacterial sulphate reduction (BSR). At MacMillan Pass, the supporting evidence for this, aside from textural interpretations (e.g. stratiform sulphides), has been in the form of sulphur isotope data obtained from bulk rock analyses of pyrite and barite (Figure 2; replotted from Goodfellow and Jonasson, 1984). There is a sizeable fractionation of sulphur isotopes during BSR (Kaplan and Rittenburg, 1964), a result of the preferential reduction of $^{34}SO_4^{2-}$ over $^{34}SO_4^{2-}$. At MacMillan Pass, enrichments of ^{34}S in bedding paralle pyrite and barite are cited as evidence for basinal restriction and near quantitative reduction of seawater sulphate via BSR (Goodfellow and Jonasson, 1984). This model, it should be emphasized, is predicated on the assumption that reduced sulphur was generated almost exclusively by BSR in closed-system conditions, and that pyrite and barite formed coevally from a euxinic water column.

However, recent petrographic work has demonstrated that sulphide and barite mineralization is not strictly stratiform, rather stratabound, and thus could have originated below the sediment-water interface (SWI) (Magnall et al., 2014). It is possible that the diagenetic history of many of these samples was more complex, with multiple generations of barite and pyrite. Using bulk analytical techniques these details cannot be resolved, and there is the risk that the isotopic data, previously from bulk-sample analysis, represents a mixture of multiple generations of these minerals. This study presents comprehensive petrographic analysis, combined with sulphur isotope analysis of pyrite and barite, obtained using secondary ion mass spectrometry (SIMS), a micro-analytical technique that provides the necessary spatial resolution to analyse individual crystals (>15 μm). This approach offers the unique capability of being able to interpret isotopic

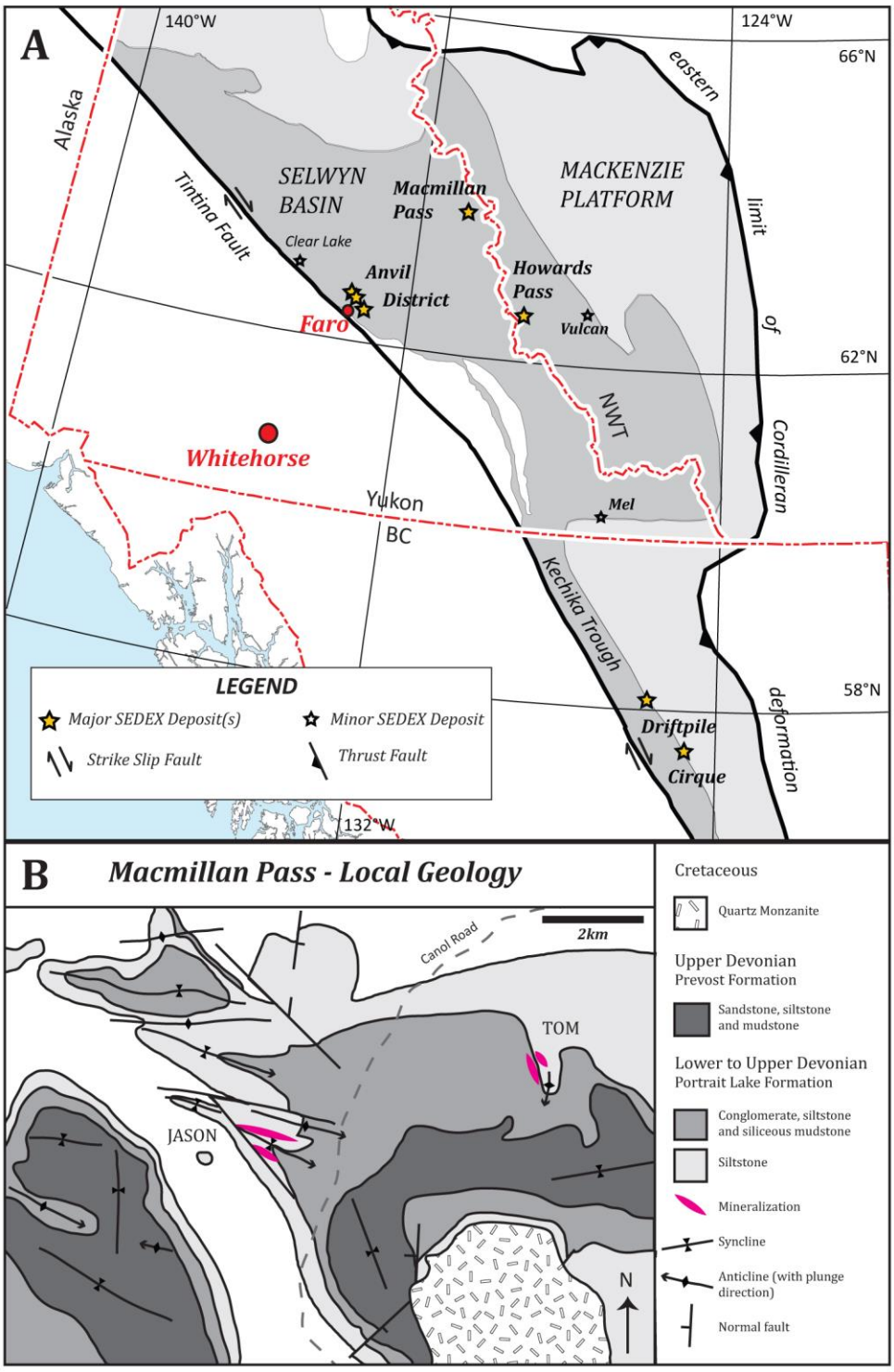

Figure 1. Regional map showing the geographical extent of the Selwyn Basin in western North America, with the location of major sediment-hosted base-metal districts highlighted (modified from Colpron and Nelson, 2011). The inset below shows the local geology of MacMillan Pass (modified from Abbott and Turner, 1990) and location of the Tom and Jason deposits.

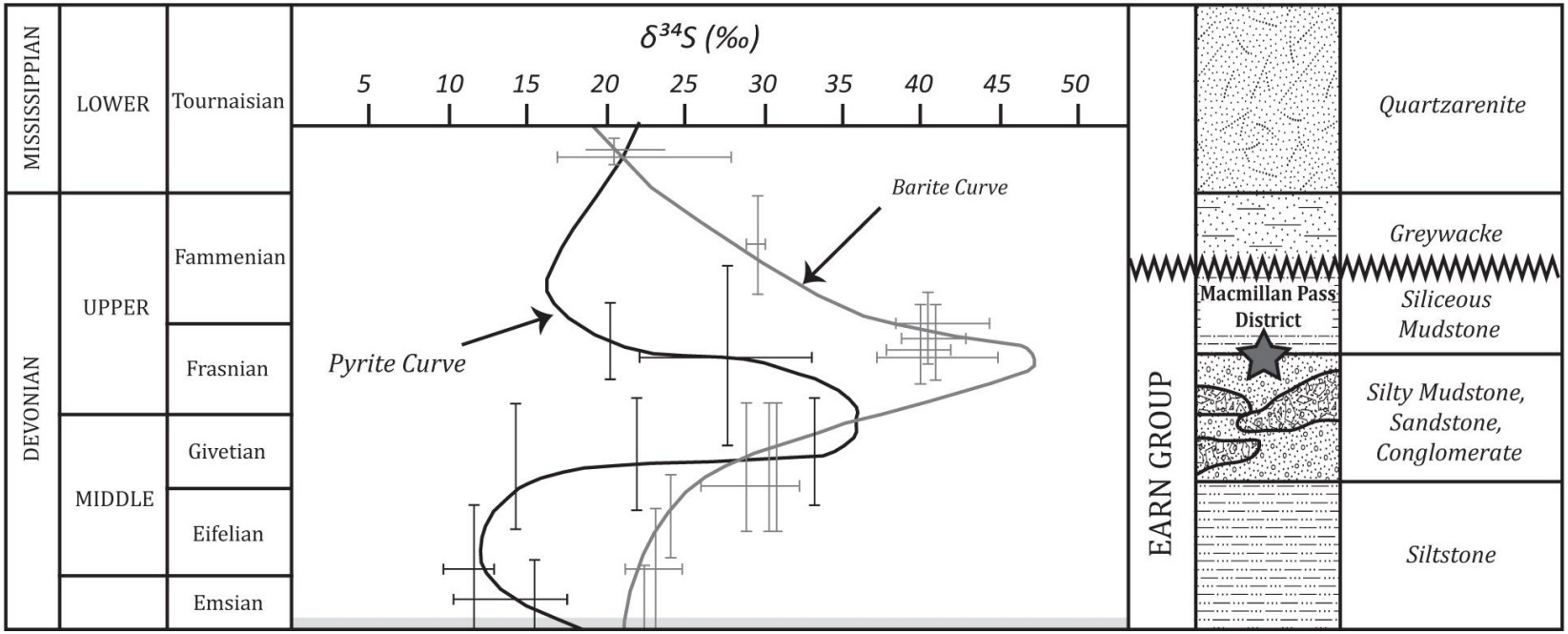

Figure 2. Late Devonian Selwyn Basin stratigraphy with the sulphur isotope curves for barite and pyrite of Goodfellow and Jonasson (1984). MacMillan Pass is denoted by the star in the Earn Group. The stratigraphy is compiled from Gordey and Anderson (1993) and Turner et al. (2011). Sulphur isotope data for barite (light grey) and pyrite (darker grey) are re-plotted from Goodfellow and Jonasson (1984).

composition in tandem with key mineralogical relationships, with the aim of evaluating the evidence for euxinia in the basin at MacMillan Pass during hydrothermal activity.

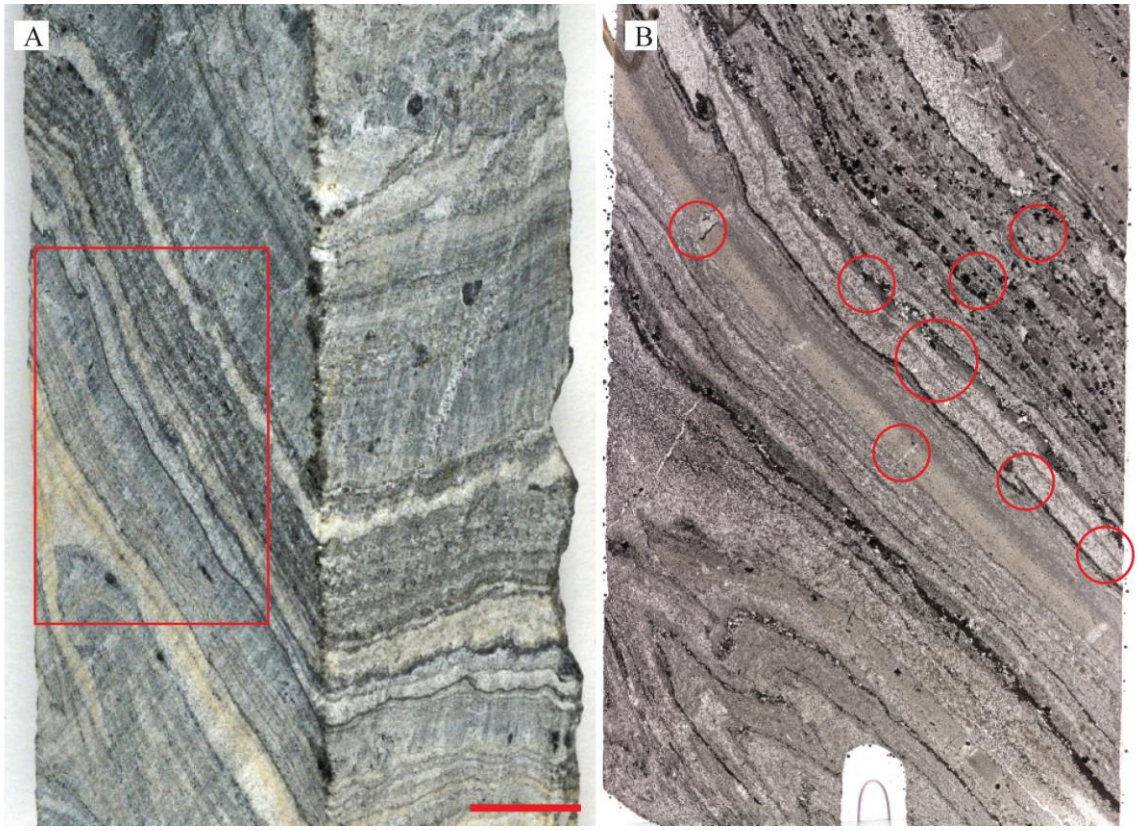

Figure 3. Photograph of a mineralized hand sample (TYK2-8) from the Tom deposit. Scale bar = 1cm. B - thin section of area in A marked by a red rectangle. Red circles indicate zones drilled out of thin section for SIMS microanalysis.

Results/Data Analysis

Methodology

Samples were collected during the summer field seasons of 2012 and 2013 from drill core stored at MacMillan Pass. Over 400 samples were collected from drill core from 10 drillholes from the Tom and Jason deposits. For the purposes of this study, care was taken to target the least deformed samples with the most representative mineralogical and textural relationships. These relationships were evaluated using a binocular microscope and transmitted and reflected light microscopy. A mineralogical paragenesis was developed on the basis of crosscutting relationships and evidence (or lack thereof) of textural equilibrium between key mineral phases.

Isotopic analysis of pyrite and barite, along with precursory sample preparation and imaging, were performed at the Canadian Centre for Isotopic Microanalysis (CCIM) at the University of Alberta, Edmonton, Canada, using a Cameca IMS-1280 ion microprobe. Samples were cored from either thin sections or rock chips using diamond core bits ranging between 2 and 3 mm diameter. The sample

cores (n = 40) were cleaned, and cast in epoxy, along with pre-polished pieces of in-house barite and pyrite reference materials (RM's) to form two standard 25mm mounts (M1269 and M1270). The mounts were coated with 30nm Au, and imaged using a Zeiss EVO MA15 Scanning Electron Microscope (SEM). Greyscale cathodoluminescence (CL) images were also acquired using the SEM.

Sulphur isotope ratios ($^{34}S/^{32}S$) and oxygen isotope ratios ($^{18}O/^{16}O$) were determined using an IMS-1280 multi-collector ion microprobe. The isotopic composition of sulphur and oxygen are reported in terms of standard δ-notation, in reference to the composition of Vienna Canyon Diablo Troilite (VCDT) for sulphur (1), and Vienna Standard Mean Ocean Water (V-SMOW) for oxygen (2);

$$\delta^{34}S \text{ ‰} = 1000\ x\ [\ (^{34}S/^{32}S)_{\text{sample}} - (^{34}S/^{32}S)_{\text{VCDT}}\ ] / (^{34}S/^{32}S)_{\text{VCDT}} \qquad (1)$$

$$\delta^{18}O \text{ ‰} = 1000\ x\ [\ (^{16}O/^{18}O)_{\text{sample}} - (^{16}O/^{18}O)_{\text{VSMOW}}\ ] / (^{16}O/^{18}O)_{\text{VSMOW}} \qquad (2)$$

Key analytical parameters are summarized in Table 1. The primary beam used focused 20 keV $^{133}Cs^+$ ions to form a probe (diameter and beam current; Table 1). Rastering of the primary beam (area; Table 1), for 60 s prior to analysis, cleared the surface of contaminants and implanted Cs. The normal incidence electron gun was utilized for analysis of barite. Isotopes of interest ($^{32}S^-$, $^{34}S^-$, $^{16}O^-$, $^{18}O^-$) were analyzed simultaneously in Faraday cups (L'2 using $10^{10}\ \Omega$ amplifier, and FC2 or H'2 with $10^{11}\ \Omega$, respectively); see Table 1 for mass resolutions and mean count rates. Analyses of unknowns were interspersed with the RM's in a 4:1 ratio. Instrumental mass fractionation (IMF) was determined for each analytical session from utilizing all the replicate analyses of the RM's. Final uncertainties are typically ±0.20 to 0.25 ‰ (Table 1) at 95% confidence interval (2σ), and propagate within-spot counting errors, between-spot errors (geometric effects) and between-session errors. Errors do not include the absolute uncertainty in the composition of the RMs (Table 1) of ±0.2 to 0. 5 ‰. No orientation-related biases have been found for SIMS analysis of pyrite or barite at CCIM (e.g. Kozdon et al., 2010). During the analytical sessions, a total of 176 $\delta^{34}S$ analyses of pyrite were performed, and 184 $\delta^{34}S$ and 121 $\delta^{18}O$ analyses of barite.

Petrography

Three pre-mineralization generations of barite are recognized; (1) *barite-I* occurs as small (<25μm) interstitial, anhedral crystals that form enrichments along and within individual mudstone laminae (Figure 4A), (2) *barite-II* forms a distinctive, commonly patchy replacement of mudstone (Figure 4B and C), but also occurs as equant, euhedral crystals in mono-minerallic stratiform laminations (Figure 4A), and discontinuous stratabound enrichments, (3) *barite-III* is present within irregular veinlets that cross-cut mudstone laminae and earlier generations of barite (Figure 4A). All three generations of barite formed before hydrothermal input and precipitation of sphalerite, galena and hydrothermal pyrite.

	δ^{34}S-pyrite	δ^{34}S-barite	δ^{18}O-barite
Cs probe diameter (μm)	10	15	12
Beam Current (nA)	0.85	2.5	2.5
Electron gun used	no	yes	yes
Implantation raster (μm)	18 x 18	20 x 20	20 x 20
Entrance & field apertures (μm, mm)	122, 5x5	122, 5x5	122, 5x5
Field magnification	100x	100x	100x
Energy slit	Full open	Full open	Full open
Detectors	L'2 (FC, $10^{10}\Omega$), FC2 (FC, $10^{11}\Omega$)	L'2 (FC, $10^{10}\Omega$), FC2 (FC, $10^{11}\Omega$)	L'2 (FC, $10^{10}\Omega$), H'2 (FC, $10^{11}\Omega$)
Mass Resolution	2000, 2100	2000, 2100	1950, 2275
Secondary ions detected and mean counts/s	$^{32}S^- = 1*10^9$ $^{34}S^- = 4.5*10^7$	$^{32}S^- = 7*10^8$ $^{34}S^- = 3*10^7$	$^{16}O^- = 3.5*10^9$ $^{18}O^- = 7*10^6$
RM identity	S0322A pyrite	S0327 barite	S0327 barite
RM composition	$\delta^{34}S_{VCDT}$ = -0.2 ± 0.2‰	$\delta^{34}S_{VCDT}$ = +22.3 ± 0.5‰	$\delta^{18}S_{VSMOW}$ = +11.0 ± 0.5‰
Peak counting time	75 s	75 s	75 s
Standard deviation of RM analyses	0.04‰	0.05‰	0.07‰ – 0.11‰
Typical ±2σ of unknowns	± 0.17‰	± 0.18‰	± 0.24‰

Table 1. Key analytical parameters

Two principal pre-mineralization generations of pyrite include: (1) *pyrite-I* is framboidal, mostly 10-20 μm in diameter (Figure 5A), (2) *pyrite-II* is euhedral, and forms either stratiform accumulations (Figure 5B) of euhedral pyrite (*pyrite-IIa*) or individual idiomorphic crystals (*pyrite-IIb*), which often occur within *barite-II* (Figure 5C). These two sub-generations of *pyrite-II* are associated with different δ^{34}S compositions (see below). Both *pyrite-I* and *pyrite-II* are present within samples from the stratabound mineralization, and also unmineralized mudstone samples.

Hydrothermal pyrite (*pyrite-III*) can be found in association with sphalerite and galena. It occurs as large, sub- to anhedral replacements and overgrowths of earlier-formed barite (Figure 5D), in a mineral assemblage with witherite and sphalerite. Galena is the last phase to form in the paragenesis, and occurs as anhedral, interstitial crystals that overprint earlier barite and pyrite along

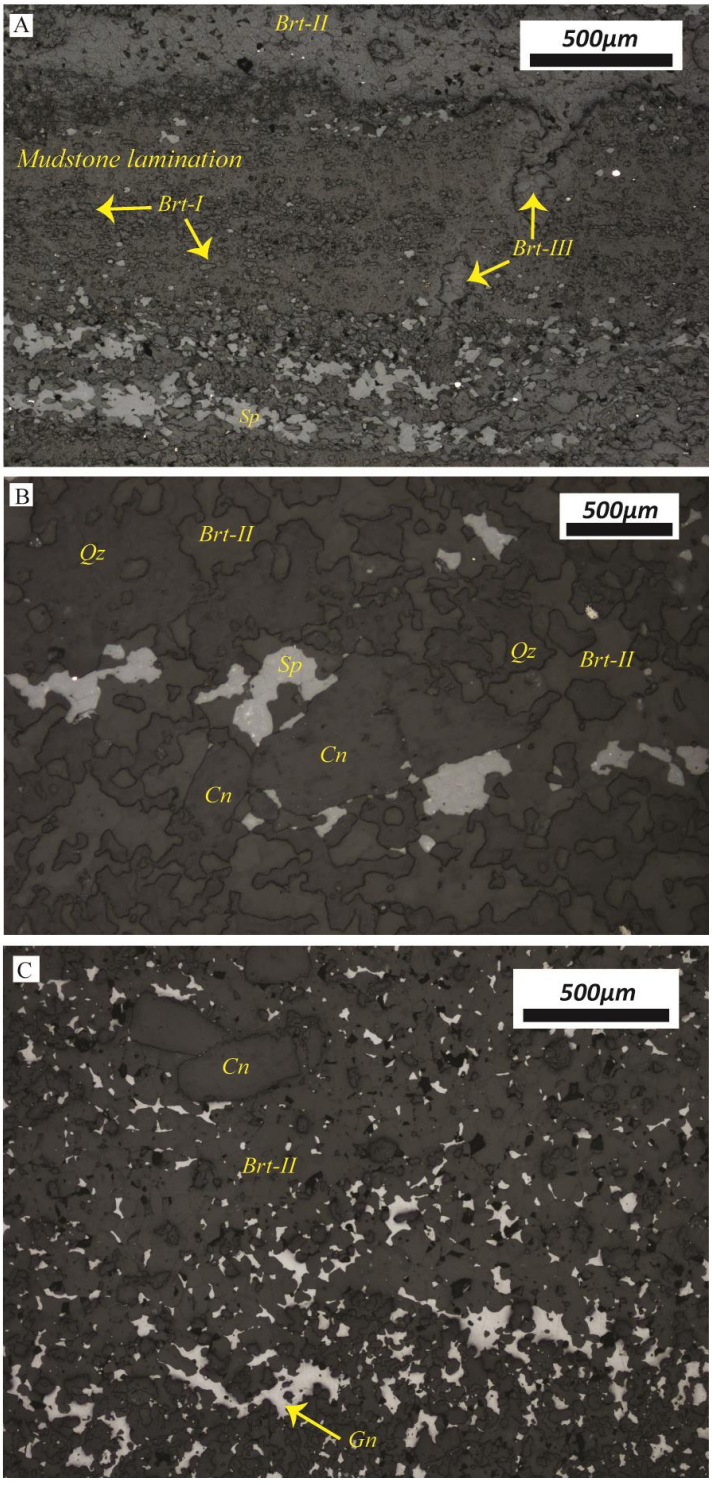

Figure 4. Photomicrographs in reflected light of: A - mudstone lamination with interstitial barite (Brt-I), interlaminated with Brt-II and cut by Brt-III. Sphalerite replaces barite towards bottom of the image. B - interstitial barite (Brt-II) in microcrystalline quartz (Qz). Barium feldspar (celsian; Cn) occurs in the centre of the image, partially replaced by barite. Sphalerite (Sp) occurs as interstital replacement of barite. C – interstitial replacement of *barite-II* by galena (Gn).

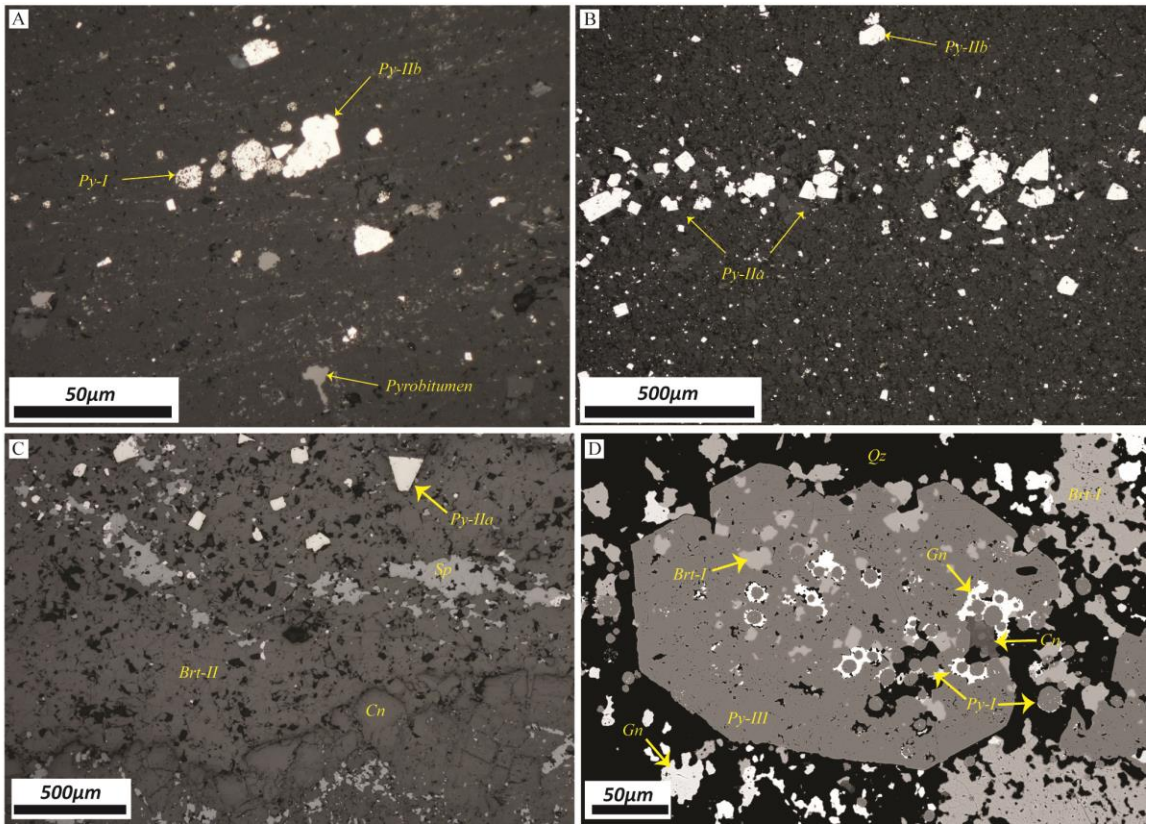

Figure 5. Photomicrographs in reflected light of: A - framboidal *Py-I* overgrown by euhedral *pyrite-IIb*, in a siliceous mudstone with interstitial pyrobitumen. B - *pyrite-IIa,* concentrated along a bedding parallel horizon. C - barium feldspar (celsian; Cn) precipitated along a stratal horizon, overlying and replaced by equant, euhedral barite (*Brt-II*). *Barite-II* is associated with euhedral pyrite crystals (Py-IIa), and both are replaced by subsequent sphalerite (Sp). D - backscatter electron image Of framboidal pyrite (*Py-I*) and barite (*Brt-I*) overprinted by later generation of pyrite (*Py-III*); framboidal pyrite seems to provide a porous framework for the mineralizing fluid to exploit, highlighted by the precipitation of galena.

stratiform layers (Figure 4C). Sphalerite and galena appear to precipitate and replace barite at triple-point junctions of crystals, leading to the development of anhedral, interstitial crystals within more euhedral barite.

Sulphur Isotopes

The sulphur isotope compositions of all generations of pyrite and barite are compiled in Figure 6. *Pyrite-I* has a distinctive isotopic composition, with $\delta^{34}S$ values between -28‰ and -15‰. Subsequent generations of pyrite (*pyrite-II + III*) overlap in isotopic composition, with a wide range of $\delta^{34}S$ values between 3‰ and 28‰. Barite, in contrast to pyrite, has a much narrower range of $\delta^{34}S$ composition, with values ranging between 24‰ and 34‰, and a median of 27‰. There are notable small-scale $\delta^{34}S$ variations, between barite crystals less than 50µm from each other, on the order of 3-4‰.

Discussion/Models

Textural Relationship of Barite and Pyrite

At the Tom and Jason deposits, there are some important mineralogical relationships that have not been documented in previous studies: (1) in all samples, barite pre-dates the ore forming sulphides (galena, sphalerite and *pyrite-III*); (2) there are multiple generations of barite, including vein barite (*barite-III*), which suggests that barium underwent remobilization within the host-rock; and (3) there are multiple generations of pyrite, including two that formed prior to Zn-Pb sulphide mineralization.

The mineralogy of these MacMillan Pass systems, although simple (pyrite – sphalerite – galena ± barite), is clearly complicated in terms of its temporal development. There are multiple generations of barite and pyrite that precede the main hydrothermal event, and only *barite-II* and *pyrite-IIb* formed coevally (Figure 5C). *Pyrite-III*, which was associated with hydrothermal input, shows clear disequilibrium textures with respect to earlier-formed barite and pyrite (Figure 5D). Therefore, in terms of bulk analyses, it is clear that previous sulphur isotope data (Goodfellow and Jonasson, 1984) represent a mixture of the isotopic compositions from multiple generations of barite and pyrite. Furthermore, at the micro-scale, there is minimal evidence of truly synsedimentary, laminated base metal sulphide precipitation (Magnall et al., 2014). It is therefore necessary to re-evaluate the isotopic evidence for basinal euxinia.

$\delta^{34}S$ Composition of Barite

The lowest $\delta^{34}S_{\text{-barite}}$ values (24‰) overlap with carbonate-associated sulphate (CAS) constraints on the $\delta^{34}S$ composition of Late Devonian seawater (John et al., 2010; Chen et al., 2013). This suggests that, with respect to sulphate at least, the Selwyn Basin was not restricted from circulation with the global oceans during hydrothermal activity. Furthermore, we have not found any extremely positive $\delta^{34}S_{\text{-barite}}$ values, which would support a model involving a Rayleigh sulphate reduction scenario in a closed system. Indeed, the narrow range in $\delta^{34}S_{\text{-barite}}$ is more typical of sulphate modified by BSR in open-system conditions, where sulphate resupply is greater than sulphate reduction.

Within the barite paragenesis, there is overlap in the $\delta^{34}S$ composition of different generations of barite, which likely means barite formed from fluids that had a similar source of sulphate. Using the criteria of Paytan et al. (2002), there is limited textural evidence for syn-sedimentary precipitation of barite; instead, the vast majority of barite is more consistent with formation below the sediment/water interface (SWI), in a diagenetic environment. The $\delta^{34}S$ composition of barite supports this conclusion, albeit in a diagenetic environment that is well connected with overlying seawater (perhaps 10 to 100 cm beneath the SWI), such that open-system conditions are maintained.

$\delta^{34}S$ Composition of Pre-mineralization Pyrite

The $\delta^{34}S$ isotopic composition of *pyrite-I* represents a large fractionation from Late Devonian seawater sulphate ($\Delta_{\text{-sulphate-sulphide}}$ = 49‰), and is consistent with slow rates of BSR (Goldhaber and Kaplan, 1975). As with $\delta^{34}S_{\text{-barite}}$, the range of $\delta^{34}S_{\text{-Py-I}}$ values we report are consistent with precipitation by BSR from the same diagenetic seawater pore fluid. The isotopic composition of barite and *pyrite-I* is not unique to formation from a system undergoing closed-system Rayleigh fractionation, and there is no evidence from the $\delta^{34}S$ analyses of barite that sulphate was reduced in near quantitative proportions. The relationship between barite and pyrite-I, whereby a large isotopic fractionation between $\delta^{34}S_{\text{-sulphate}}$ and $\delta^{34}S_{\text{-sulphide}}$ is preserved, is typical of BSR in normal marine mudstones (e.g. Canfield, 2004). The diameter of the framboidal pyrite analysed in this study (>7 µm) is also consistent with diagenetic pyrite formation, as opposed to precipitation from a euxinic water column (Wilkin et al., 1996).

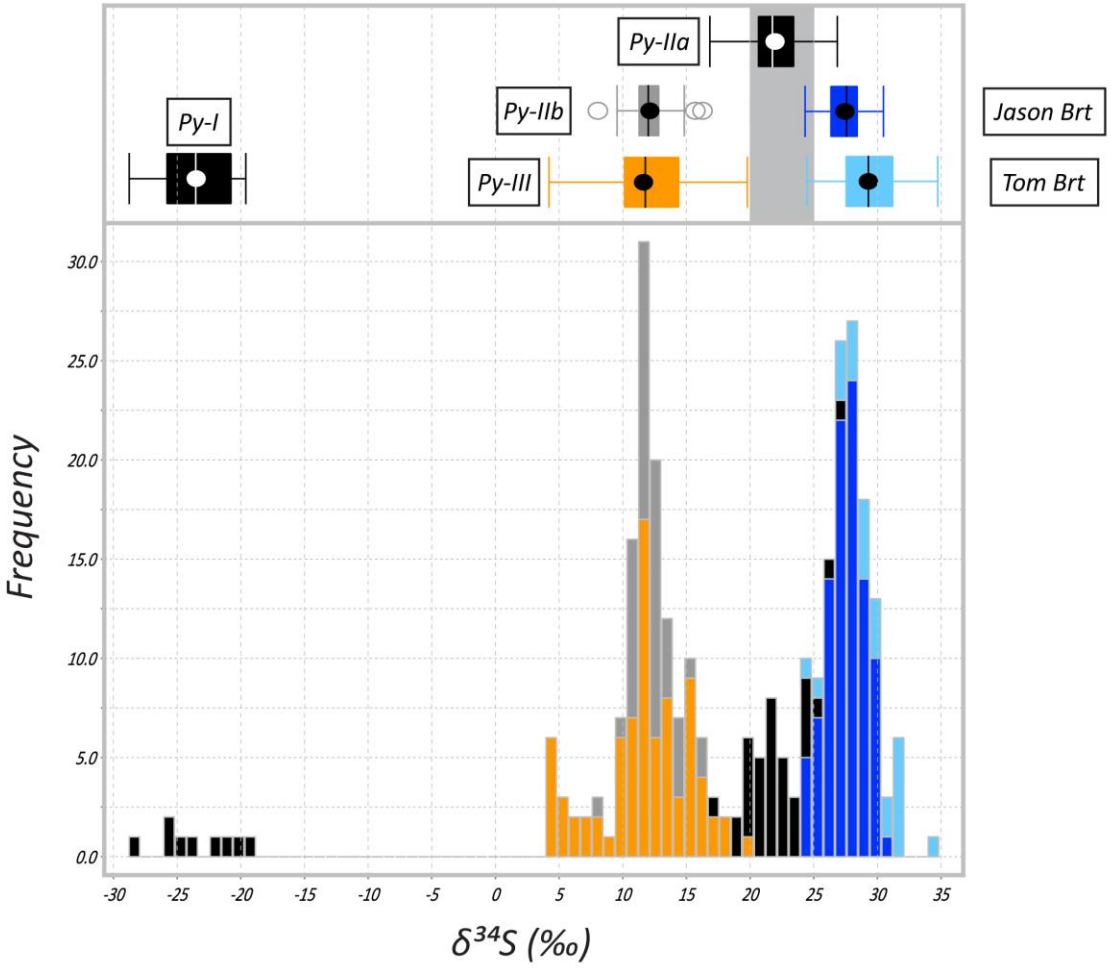

Figure 6. Histogram of compiled $\delta^{34}S$ results for entire study. Above the histogram are box and whisker representations summarizing the data in the histogram, along with labels. The grey box represents the $\delta^{34}S$ range of Frasnian seawater (John et al., 2010; Chen et al., 2013). Median values = vertical line; mean = circle; black box = interquartile (Q1 to Q3) range (IQR); lines extend to Q-n +(1.5*IQR) and circles outside lines are outliers.

Pyrite-II forms a distinct contrast to *pyrite-I*, both in morphology and $\delta^{34}S$ composition. In some cases, the $\delta^{34}S_{\text{-pyrite-II}}$ composition approaches coeval seawater sulphate ($\delta^{34}S \cong 24‰$; Figure 6) and the values reported by Goodfellow and Jonasson (1984). However, *pyrite-II* is also the only pyrite formed in direct association with barite, and in some cases (*pyrite-IIb*) textural equilibrium is observed (Figure 5C). The $\delta^{34}S$ composition of barite therefore forms an important constraint for interpreting the isotopic composition of pyrite. In particular, the $\delta^{34}S_{\text{-barite}}$ reflects the isotopic composition of unmodified Late Devonian seawater sulphate. Therefore, the positive $\delta^{34}S$ values recorded by *pyrite-II* cannot have been generated during the development of euxinic conditions. The end members that *pyrite-1* and *pyrite-II* form in terms of $\delta^{34}S$ composition, and their textural differences (crystal morphology, mineralogical relationship with barite), suggest a complex diagenetic history, and perhaps one in which reduced sulphur was produced by different processes. Importantly, these isotopic signatures were developed prior to hydrothermal input, in a diagenetic environment. Processes operating beneath the SWI, and not in the water column (i.e. euxinia), must have formed the metal trap in order to account for the accumulation of base metal sulphides in the strata at MacMillan Pass.

$\delta^{34}S$ Composition of Hydrothermal Pyrite

Pyrite-III displays a broad range in $\delta^{34}S$ composition (~4‰ to 20‰). The interquartile range (Q1 to Q3; *Pyrite-III*) overlaps with *Pyrite-IIb*, but also extends to lower and higher values of $\delta^{34}S$, and likely represents mixing of reduced sulphur from multiple sources. There is abundant textural evidence for barite dissolution and replacement by pyrite (Figure 7), and so one potential sulphur source would be the recycling of barite-sulphur by the hydrothermal fluid. In all samples, barite clearly pre-dates hydrothermal input. Figure 7 provides an example of a mineral assemblage that is commonplace in the mineralization at Tom and Jason, involving witherite-pyrite-sphalerite associated with barite dissolution. Witherite ($BaCO_3$) will only precipitate from high barium—low sulphate fluids (Hanor, 2000), and so is a likely by-product of barite dissolution coupled with sulphide precipitation. Barite replacement has been identified as a potential mechanism for sulphide precipitation at Red Dog, the world class Pb-Zn-Ba deposit (Kelley et al., 2004), however this is the first time it has been recognized at MacMillan Pass. However, it should be emphasized that the distribution of $\delta^{34}S$ values in *pyrite-III* is not consistent with quantitative recycling of barite-sulphur, and the broad range of values may reflect the mixing of the hydrothermal fluid with reduced sulphur in the diagenetic fluids, derived from other sources.

Implications for Exploration

The primary conclusion of this study is that euxinic conditions do not form a prerequisite for sediment-hosted base metal mineralization at MacMillan Pass. The $\delta^{34}S$ composition of barite provides no evidence that seawater sulphate underwent near quantitative reduction in the water column. This has important implications for the generation of base metal sulphide enrichments in Selwyn

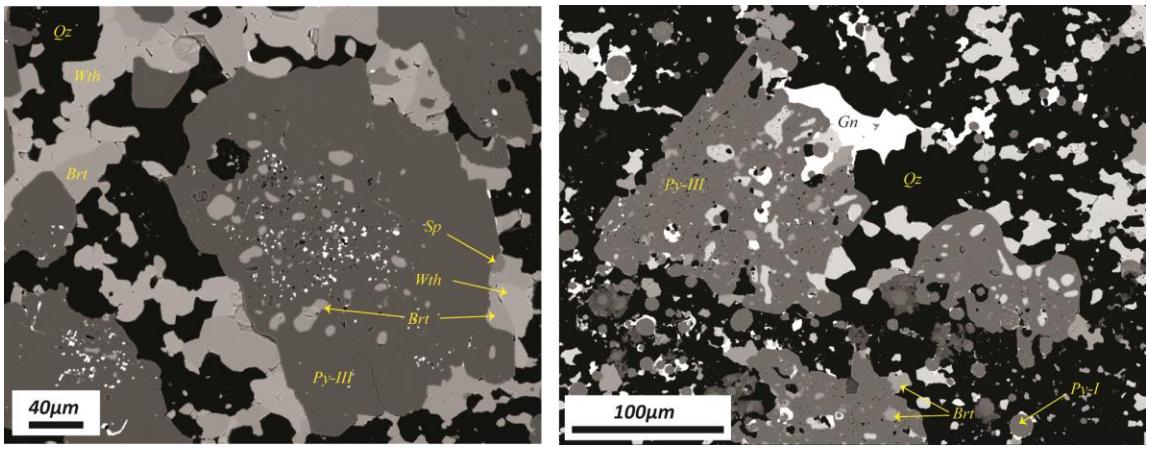

Figure 7. A – barite (Brt) dissolution association with sphalerite (Sp), witherite (Wth) and *Py-III* overgrowth. B – *Py-III* and galena (Gn) overprinting barite intergrown with quartz (Qz).

Basin strata. Although it does not rule out euxinia in other Selwyn Basin systems (Anvil District, Howards Pass), it does clearly show that positive excursions in the $\delta^{34}S_{\text{-pyrite}}$ record are not unique to the development of euxinic conditions, but can also be formed during diagenesis. At MacMillan Pass, this means that alternative sources of sulphur are required to account for base metal sulphide deposition; one such mechanism is barite replacement, and from an exploration perspective in Late Devonian strata, barite enrichments may represent fertile host-rocks for base metal sulphide enrichments. The relationship between barite enrichments and conduits for hydrothermal fluid flow (extensional fault systems) is likely to be an important control on the development of hydrothermal systems.

Future Work

There are two main components to the planned future work: (1) given the importance of pre-existing barite enrichments in the strata at MacMillan Pass what processes may be responsible for barite accumulation? Further analysis of barite, focusing on the oxygen isotope composition ($\delta^{18}O$) of barite-sulphate, will likely provide valuable information; and (2) the geochemical conditions under which sulphur is transformed from sulphate in barite to sulphide in galena, sphalerite and pyrite warrants further evaluation. Once the temperature and salinity of the hydrothermal fluid has been established (fluid inclusion studies), using geochemical modelling it will be possible to evaluate the conditions in which sulphide precipitation proceeds via barite replacement. In addition, the $\delta^{34}S$ composition of galena and sphalerite from mineralization at MacMillan Pass will be documented by in situ techniques (SIMS), which will provide important constraints on how sulphur isotopes are fractionated during barite replacement.

Acknowledgements

We would like to thank the Geological Survey of Canada, and specifically the TGI-4 initiative for funding this study, and Hudbay Mineral Resources for access to the drill core and camp at MacMillan Pass. Sample preparation for SIMS analysis was greatly assisted by Anna Oh.

References

Abbott, J.G., and Turner, R.J.W., 1990, Character and paleotectonic setting of Devonian stratiform sediment-hosted Zn-Pb-barite deposits, MacMillan Fold Belt, Yukon, *in* Abbott J.G., Turner R.J.W., ed., Mineral deposits of the northern Canadian Cordillera: Ottawa, International Association on the Genesis of Ore Deposits, Eighth Symposium, Field Trip 14 Guidebook, p. 99-136.

Canfield, D.E., 2004, The evolution of the earth surface sulfur reservoir: American Journal of Science, v. 304, p. 839-861.

Chen, D., Wang, J., Racki, G., Li, H., Wang, C., Ma, X., and Whalen, M.T., 2013, Large sulphur isotopic perturbations and oceanic changes during the Frasnian-Fammenian transition of the Late Devonian: Journal of the Geological Society, London, v. 170, p. 465-476.

Colpron, M., and Nelson, J.L., 2011, A digital atlas of terranes for the Northern Cordillera. geology.gov.yk.ca

Goldhaber, M.B., and Kaplan, I.R., 1975, Controls and consequences of sulfate reduction rates in recent marine sediments: Soil Science, v. 119, p. 42-55.

Gordey, S.P., Abbott, J.G., and Orchard, M.J., 1982, Devono-Mississippian Earn Group and younger in strata in east-central Yukon: Current Research, Part B; Geological Survey of Canada, Paper 82-1B, p. 93-100.

Gordey, S.P., and Anderson R.G., 1993, Evolution of the northern cordilleran miogeocline, Nahanni map area (105I), Yukon and Northwest Territories: Geological Survey of Canada, Memoir, v. 428, 214 p.

Goodfellow, W.D., and Jonasson, I.R., 1984, Ocean stagnation and ventilation defined by secular trends in pyrite and barite, Selwyn Basin, Yukon: Geology, v. 12, p. 583-586.

Goodfellow, W.D., and Lydon, J.W., 2007, Sedimentary exhalative (SEDEX) deposits, *in* Goodfellow, W.D., ed., Mineral deposits of Canada: A synthesis of major deposit types, district metallogeny, the evolution of geological provinces, and exploration methods: Geological Association of Canada, Mineral Deposits Division, Special Publication no. 5, p. 163-183.

Goodfellow, W.D., 2007, Base Metallogeny in the Selwyn Basin, Canada, *in* Goodfellow, W.D., ed., Mineral deposits of Canada: A synthesis of major deposit types, district metallogeny, the evolution of geological provinces, and exploration methods: Geological Association of Canada, Mineral Deposits Division, Special Publication no. 5, p. 553-579.

Goodfellow, W.D., and Rhodes, D., 1990, Geological setting, geochemistry and origin of the Tom stratiform Zn-Pb-Ag-barite deposits: *in* Abbott, J.G., and Turner, R.J.W., ed., Mineral deposits of the northern Canadian Cordillera: Ottawa, International Association on the Genesis of Ore Deposits, 8th symposium, field trip 14 guidebook, p. 177-244.

Hanor, J.S., 2000, Barite-Celestine Geochemistry and Environments of Formation: Reviews in Mineralogy and Geochemistry, v. 40, p. 193-275.

John, E.H., Wignall, P.B., Newton, R.J., and Bottrell, S.H., 2010, $\delta^{34}S_{CAS}$ and

$\delta^{18}O_{CAS}$ records during the Frasnian-Fammenian (Late Devonian) transition and their bearing on mass extinction models: Chemical Geology, v. 275, p. 221-234.

Kelley, K.D., Leach, D.L., Johnson, C.A., Clark, J.L., Fayek, M., Slack, J.F., Anderson, V.M., Ayuso, R.A., and Ridley, W.I., 2004, Textural, compositional, and sulfur isotope variations of sulphide minerals in the Red Dog Zn-Pb-Ag deposits, Brooks Range, Alaska: Implications for ore formation: Economic Geology, v. 99, p. 1509-1532.

Magnall, J.M., Gleeson, S.A., and Paradis, S., 2014, SEDEX mineralisation, MacMillan Pass (YT): Petrography, mineralogy and bulk geochemistry of the Tom and Nidd deposits: Geological Survey of Canada, Open File 7457, 19 p.

Paytan, A., Mearon, S., Cobb, K., and Kastner, M., 2002, Origin of marine barite deposits: Sr and S isotope characterization: Geology, v. 30, no. 8, p. 747-750.

Turner, E.C., Roots, C.F., MacNaughton, R.B., Long, D.G.F., Fischer, B.J., Gordey, S.P., Martel, E., and Pope, M.C., 2011, Stratigraphy, *in* Martel, E., Turner, E.C., and Fischer, B.J. ed., Geology of the central Mackenzie Mountains of the northern Canadian Cordillera, Sekwi Mountain (105P), Mount Eduni (106A), and northwestern Wrigley Lake (95M) map-areas, Northwest Territories: Special Volume 1, Northwest Territories Geoscience Office, p. 31-192.

Wilkin, R.T., Barnes, H.L., and Brantley, S.L., 1996, The size distribution of framboidal pyrite in modern sediments: an indicator of redox conditions: Geochimica et Cosmochimica Acta, v. 60, p. 3897-3912.